

Document downloaded from:

<http://hdl.handle.net/10251/105532>

This paper must be cited as:

Liu, L.; Díaz Morales, UM.; Arenal, R.; Agostini, G.; Concepción Heydorn, P.; Corma Canós, A. (2017). Generation of subnanometric platinum with high stability during transformation of a 2D zeolite into 3D. *Nature Materials*. 16(1):132-138. doi:10.1038/NMAT4757



The final publication is available at

<https://doi.org/10.1038/NMAT4757>

Copyright Nature Publishing Group

Additional Information

Generation of subnanometric platinum with high stability during transformation of two-dimensional into three-dimensional zeolite

Lichen Liu,¹ Urbano Diaz,¹ Raul Arenal,^{2,4} Giovanni Agostini,³ Patricia Concepcion¹ and Avelino Corma^{1*}

¹ *Instituto de Tecnología Química, Universitat Politècnica de València-Consejo Superior de Investigaciones Científicas (UPV-CSIC), Av. de los Naranjos s/n, 46022 Valencia, Spain*

² *Laboratorio de Microscopias Avanzadas, Instituto de Nanociencia de Aragon, Universidad de Zaragoza, Mariano Esquillor Edificio I+D, 50018 Zaragoza, Spain*

³ *European Synchrotron Radiation Facility, 6 Rue Jules Horowitz, Grenoble, BP 156, F-38042, France*

⁴ *ARAID Foundation, 50018 Zaragoza, Spain*

* **Email:** acorma@itq.upv.es

The applications of single atoms and clusters for heterogeneous catalysis have attracted much attention due to the special catalytic properties of single atoms and clusters. However, the generation of stable single atoms and clusters on a solid support is still challenging. Herein, we report a new strategy for the generation of single Pt atoms and Pt clusters with exceptional high thermal stability in purely siliceous MCM-22 during the transformation of a two-dimensional into a three-dimensional zeolite. Those subnanometric Pt species are still stabilized by MCM-22 after treatment in air at 540 °C. Furthermore, Pt species confined in the internal cavities show size-selective catalytic properties in the hydrogenation of alkenes. Reduction-oxidation treatments at temperature as high as 650 °C result in the growth of Pt to still small nanoparticles between 1~2 nm. The stability and catalytic activity of Pt species is also reflected in the dehydrogenation of propane to propylene.

Introduction

The unique catalytic properties of metal cluster catalysts have attracted great attention because of their distinct behavior compared with metal nanoparticles (NPs) and mononuclear metal compounds.^{1,2} However, the stability of metal clusters can be a limitation for their applications in heterogeneous catalysis at higher temperatures, and loading atomic dispersed metal species on solid supports can be a method to improve their stability.^{3,4} To this respect, because of their high thermal stability and confinement effects, zeolite materials appear as promising supports for preparing supported metal clusters.⁵ By conventional methods (such as wet impregnation and ion exchange), the location of metal species cannot always be controlled and metal NPs will usually be formed after the post-treatment. Moreover, during the reaction or during some harsh thermal treatments, active species on the external surface can aggregate to form large NPs (>5 nm), resulting in a decrease of catalytic activity.⁶⁻⁹

Recently, Iglesia et al. have developed a method to encapsulate small metal NPs into microporous cavities during the synthesis of different zeolitic materials. Different types of metal NPs with size between 1~2 nm are encapsulated into zeolites such as Sodalite (SOD), Analcime (ANA) and Gismondine (GIS).^{10,11} This method has been used, so far, for the synthesis of Al-containing zeolites and the metal nanoparticles encapsulated in those zeolites are resistant to sintering.¹² Nevertheless, in some cases, the introduction of Al into the zeolites may restrict the reaction scope of these materials because of the acidity associated to the presence of Al sites. Gates et al. have prepared single metal atoms and metal clusters (below 1 nm) confined in zeolites and performed excellent detailed characterizations on the location and atomic structure of these metal species.^{13,14} In this case, metal clusters with identified atomicity can be anchored into the pores of pure-silica zeolites, and the stability of metal clusters obtained by thermal decomposition of the metal precursor (e.g. organometallic compounds) could be an issue. In some cases, they may agglomerate even at room temperature under ambient environment. Therefore, developing a facile and sustainable method for incorporating metal clusters in high-silica zeolites with high thermal stability is still a challenge.

In this work, we present a new strategy for preparation of zeolite-confined subnanometric Pt species (single Pt atoms and Pt clusters) catalysts with high stability during transformation of two-dimensional (2D) into three-dimensional (3D) zeolite. As the starting material, we choose a pure siliceous layered precursor of MCM-22 (MWW-type zeolite)¹⁵ with the idea that during the condensation of the layered

zeolite precursor, the hemi-cages (“cups”) and cages with internal dimensions of ~ 0.7 and $\sim 0.7 \times 1.8$ nm, respectively, would entrap the subnanometric Pt species. The resultant material will be named as Pt@MCM-22. In this way, Pt individual atoms and Pt clusters will be incorporated into the “cups” and cages of MCM-22 zeolite. It will be shown that subnanometric Pt species in the cavities can differentiate reactants by size and show exceptional high thermal stability and better catalytic activity.

Results and discussions

Structural characterizations

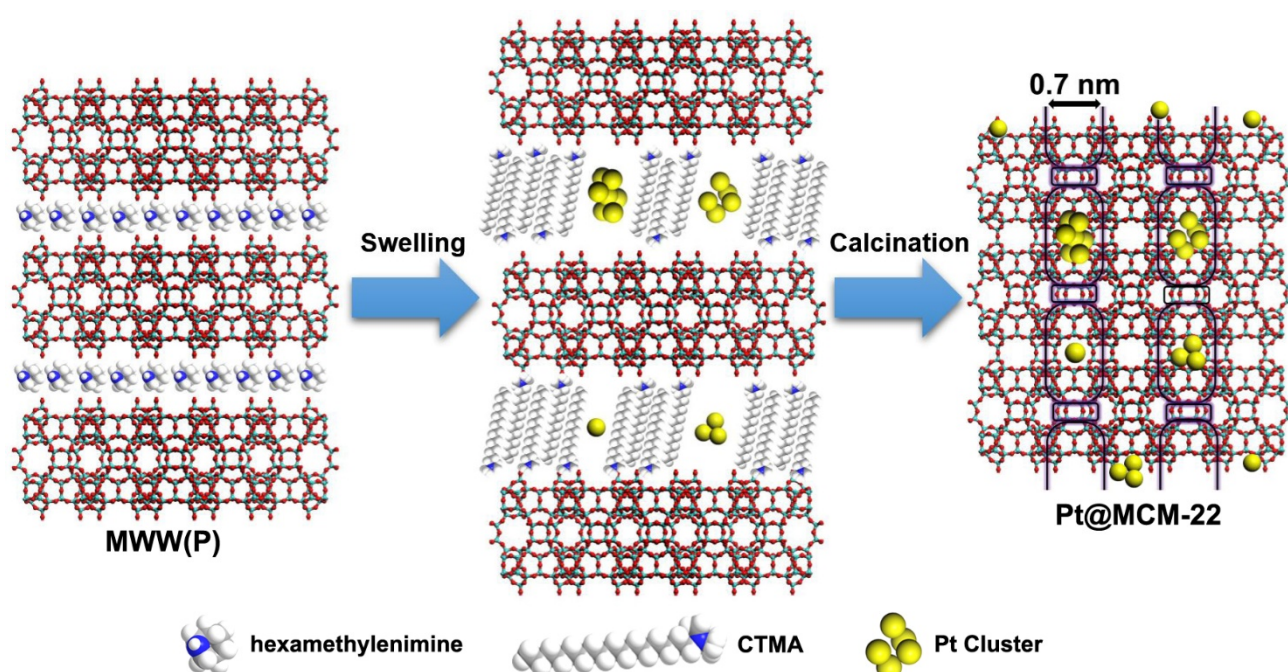


Figure 1| Schematic illustration of the preparation of Pt@MCM-22. During the swelling process of layered MWW zeolitic precursors (MWW(P)), solution containing subnanometric Pt species are added. MWW layers are expanded by the surfactant (hexadecyltrimethylammonium, CTMA^+OH^-) and subnanometric Pt species are also incorporated into the internal channels between individual MWW layers. Removing the organic agents will lead to the formation of 3D Pt@MCM-22, in which subnanometric Pt species are confined in the external “cups” on the surface or encapsulated in the supercages of MCM-22.

The preparation process of Pt@MCM-22 is schematized in **Figure 1**. In order to incorporate

subnanometric Pt species into MCM-22, purely siliceous MWW precursor (namely ITQ-1) was firstly synthesized.¹⁶ Subnanometric Pt species were prepared using dimethylformamide (DMF) as weak reduction and capping agent.^{17,18} The fluorescence emission spectrum and picture of the DMF solution containing subnanometric Pt species are shown in **Figure S1**. The incorporation of subnanometric Pt species was carried out during the swelling process of lamellar zeolitic precursor (MWW(P)), which can be followed by X-ray diffraction (see **Figure S2**). After the swelling process, subnanometric Pt species as well as the surfactant molecules were located between the layers. Then, the organic surfactant was removed by calcination in air at 540 °C, leading to formation of Pt atoms and clusters encapsulated by the supercages of 3D MCM-22, giving the final Pt@MCM-22 sample (the loading amount of Pt is 0.11 wt%, measured by ICP). Besides, Pt species could also be confined in the “cups” located at the external surface of MWW crystallites.

The structures of as-prepared Pt@MCM-22 were characterized by transmission electron microscopy (TEM) and high-resolution STEM imaging with high-angle annular dark field detector (HAADF-HRSTEM imaging). As shown in **Figure 2a**, only MCM-22 crystallites can be seen in the TEM image. The hexagonal structure of MCM-22 is preserved after the incorporation of Pt species, as confirmed by the fast Fourier transformation (FFT) and XRD patterns (**Figure S3**). In STEM images (**Figure 2b**), the 12 member-ring (MR) sub-units of the external “cups” in MCM-22 with diameter ca. 0.7 nm can be clearly seen from the view of *c*-axis. Indeed, this imaging technique is chemical sensitive because it provides Z (atomic number)-contrast between heavy Pt atoms (bright features) and MCM-22 zeolite composed by light atoms.¹⁹ The contrast for single Pt atoms have been analyzed based on the intensity profiles, as shown in **Figure 2e** and **Figure 2f**. The good dispersion of subnanometric Pt species is confirmed in additional STEM images (see **Figure S4** and **Figure S5**). Furthermore, Pt clusters and individual Pt atoms with fine dispersion can be distinguished clearly in HAADF-HRSTEM images (**Figure 2c** and **Figure 2d**). More intensity profiles of different types of Pt species can be found in supplementary information (see **Figure S6** and **Figure S7**).²⁰ It is worth mentioning that the intensity differences of the bright dots displayed in the HRSTEM-HAADF images maybe due to the focus conditions of the electron beam on the Pt atoms/clusters (or equivalently to the location, in height, of these atoms within the zeolite crystallites). For instance, **Figure 2e** (area #2) and **Figure S6** (area #3) clearly illustrate how the intensity of the dots corresponding to two neighboring atoms is

slightly different, indicating their different location in the MCM-22 crystallites. In order to better understand these findings, we have carried out HRSTEM-HAADF image simulations (see **Figure S8**). The simulation results confirm the interpretation of experimental HRSTEM images, which correspond to individual Pt atoms and Pt clusters incorporated in MCM-22. Even though it is difficult to obtain the exact location of Pt species, some important information can still be obtained based on the HRSTEM images. As shown in **Figure S9** and **Figure S10**, Pt single atoms and small clusters appear to be confined in the cups and at the connecting walls between the cups, while some Pt clusters could also be encapsulated in the supercages in MCM-22 (as illustrated in **Figure 2g**). Meantime, there are also some atomically dispersed Pt species anchored on the framework of MCM-22. Since the internal dimensions of the supercages is 0.7×1.8 nm, 10-13 Pt atoms can be contained, considering their three-dimensional structures (a schematic illustration of Pt₅ cluster confined in supercages of MCM-22 is shown in **Figure 2h**).²¹ We could only find few big Pt clusters (ca. 0.7-1.0 nm), which can fill up the supercages of MCM-22. However, there are few Pt particles larger than 2 nm which were observed in the sample.

Due to the beam sensitivity of zeolites, the location of the atoms/clusters cannot be investigated by focal-series studies.^{22,23} However, the fact that we are performing these HRSTEM-HAADF studies in an aberration-corrected microscope offers the possibility to have access to the third dimension by varying the depth of focus. As can be seen in **Figure S11**, even if the structure of MCM-22 is destroyed (including mass loss) by electron beam, Pt species still remain at the same position or just move only a few angstroms, indicating that these Pt atoms/clusters are probably embedded/anchored in the internal space of zeolite crystallites. Nevertheless, information about the location of Pt species can be deduced according to the molecular sieving effect of MCM-22, which will be discussed in the following catalytic activity section.

The particle size distribution of subnanometric Pt species shown in **Figure 2i** has been obtained by counting more than 300 particles. And a size distribution ranging from single atoms to Pt clusters nearly to 1 nm, with a majority for Pt clusters between 0.2-0.7 nm, can be seen there. It has been reported that subnanometric metal species (single atoms and clusters) are unstable above 250 °C.²⁴⁻²⁶ However, if one considers that the preparation procedure of Pt@MCM-22 includes a high-temperature process (540 °C for 4 h) for removal of organic template, it appears that subnanometric Pt species in

Pt@MCM-22 show excellent thermal stability in air.

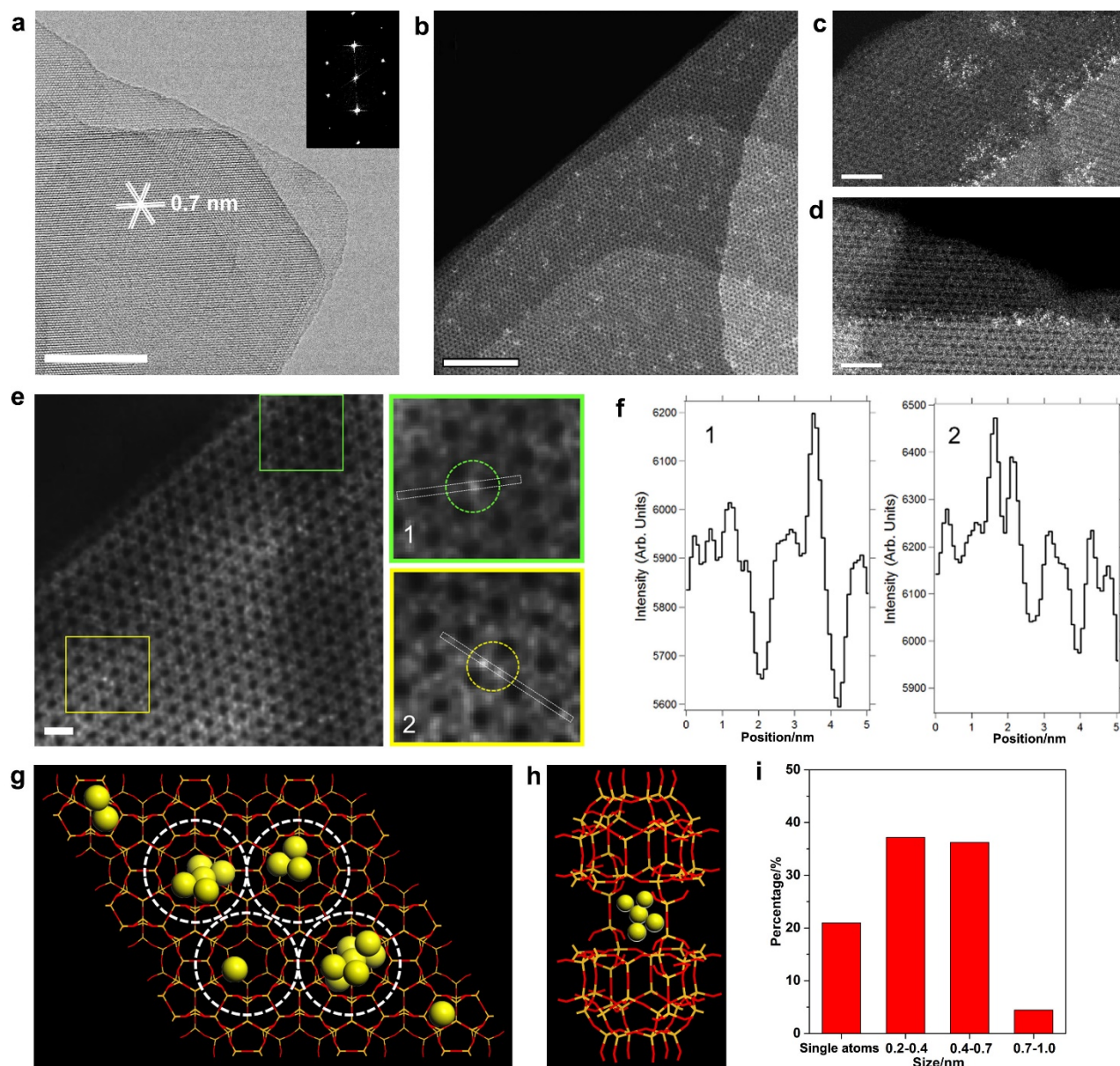


Figure 2| Atomic structures of Pt@MCM-22. **a**, TEM image of Pt@MCM-22. The insert is the corresponding FFT diffractogram of the TEM image. Scale bar, 50 nm. **b**, HAADF-STEM image of Pt@MCM-22. Scale bar, 20 nm. **c** and **d**, Atomic structures of Pt clusters confined in MCM-22. Scale bar, 5 nm. **e**, HAADF-HRSTEM image of Pt@MCM-22, where two zooms have been done in the square regions (marked in green (#1) and yellow (#2)). In these two areas, several single atoms have been highlighted. Scale bar, 2 nm. **f**, Corresponding intensity profiles obtained on the two zoomed areas. **g**, Schematic illustration of Pt@MCM-22 in a “top-down” view along the *c* axis. Pt clusters and individual Pt atoms are located in the surface cups, cavities and 12-MR supercages. **h**, Schematic

illustration of Pt₅ cluster in supercages of MCM-22. **i**, Size distribution of subnanometric Pt species in Pt@MCM-22 sample.

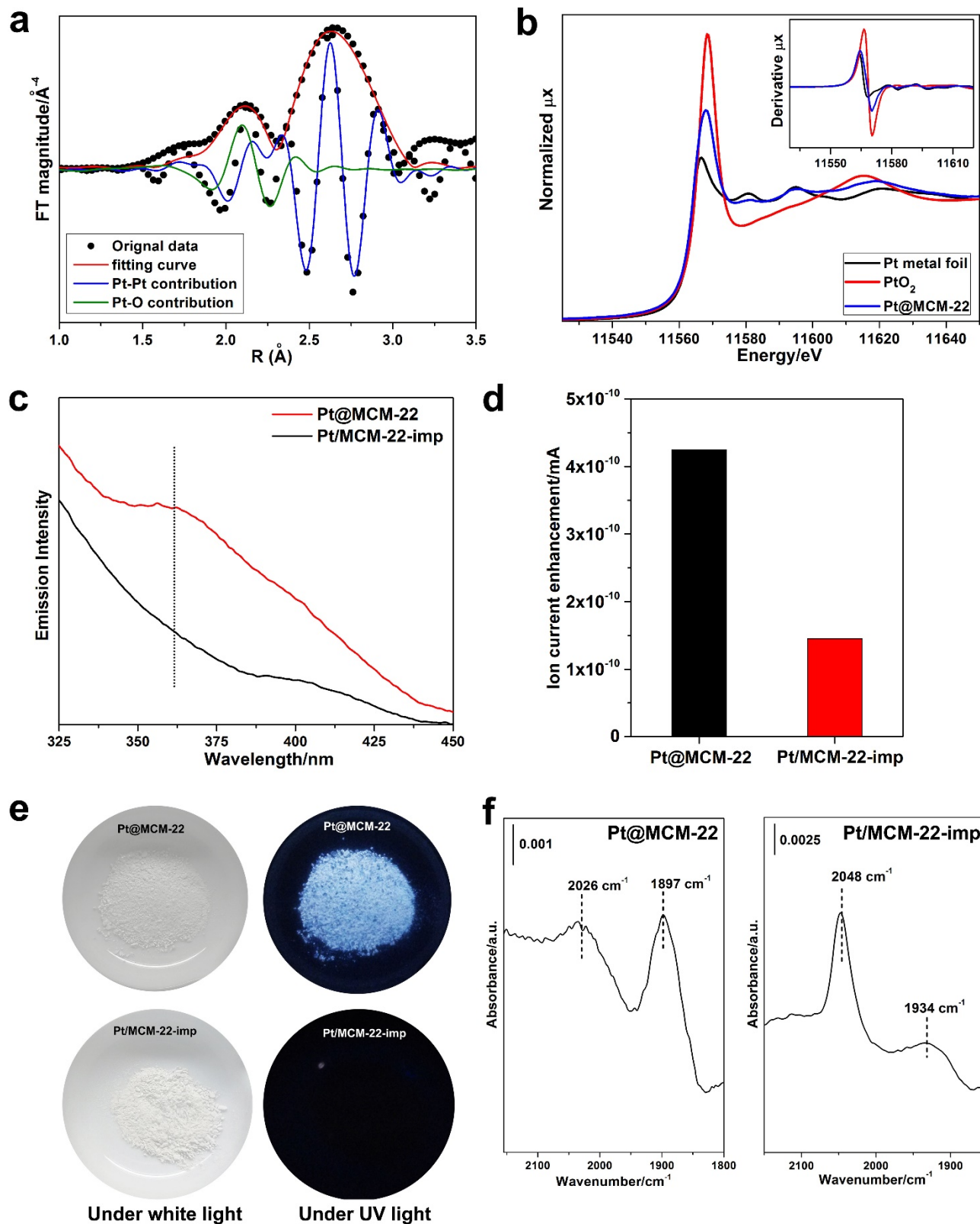


Figure 3| Characterizations of Pt@MCM-22 and Pt/MCM-22-imp. **a**, Fourier transform of k^3 -

weighted EXAFS spectrum of the Pt@MCM-22 sample (not phase-corrected). The fitting curves for Pt-O and Pt-Pt contribution are also presented. **b**, XANES spectrum of Pt@MCM-22 as well as the first-order derivative spectrum. **c**, Fluorescence emission spectra excited at 260 nm. **d**, Enhancement of the mass signal of HD in H₂-D₂ exchange experiments on Pt@MCM-22 and Pt/MCM-22-imp at room temperature. **e**, photographs of Pt@MCM-22 and Pt/MCM-22-imp under white light and UV light. **f**, IR spectra of CO adsorption on Pt@MCM-22 and Pt/MCM-22-imp.

Table 1 Result of the fit performed on **Pt@MCM-22** EXAFS spectrum

	CN	σ^2	R	E₀
Path		Å ⁻²	Å	eV
Pt-O	2.1±0.6	0.004	2.506±0.017	2.9
Pt-Pt	4.7±0.5	0.005	2.765±0.004	

$S_0^2 = 0.85$ fixed from the value extracted from the fit of the Pt foil, E_0 and ss^2 fixed from Pt foil; $\Delta k = (3.6-14.3)$ Å⁻¹ and $\Delta R = (1.4-3.5)$ Å

Spectroscopic characterization of samples

Pt@MCM-22 sample has been measured by X-ray adsorption spectroscopy (XAS) to study the local environment of Pt and to estimate the coordination numbers of Pt species. The Fourier transform of EXAFS spectra of Pt@MCM-22 and the Pt and PtO₂ reference are shown in **Figure 3a** and **Figure S12**. Considering the first shell, Pt@MCM-22 spectrum is dominated by a peak centered around 2.65 Å with a smaller contribution at 2.08 Å (both distances not phase corrected). Comparing with reference samples, the stronger contribution can be assigned to Pt-Pt bonds in Pt clusters. The assignation of weaker peak is too long to be ascribed Pt-O bonds from PtO₂ (1.65 Å, see **Figure S12**), but according to literature data it is compatible with Pt-O bonds between Pt and the zeolite frameworks.²⁷ The presence of Pt-O bonds in Pt@MCM-22 sample has also been confirmed by the XANES spectrum of Pt@MCM-22. As it can be seen in **Figure 3b**, the curve shape of Pt@MCM-22 sample looks like Pt(0) (first derivative and oscillations around 11580 and 11595 eV) but white line intensity is higher, indicating the presence of Pt-O bonds.²⁵ Based on the fitting results of the EXAFS spectrum (see **Table 1**), the coordination number of Pt in Pt@MCM-22 is ca. 4.7, that would correspond to Pt clusters with size less than 0.7 nm (i.e. with less than 13 atoms), assuming that Pt clusters show cubo-octahedral shape.^{28,29} Even though the atomicity of Pt species obtained based on EXAFS data is slightly larger than that obtained based on HRSTEM images, the average size is still in the cluster size range (below

0.7 nm), which is in line with the results obtained from electron microscopy and our synthesis principle.

As it is well known, the optical properties of metal clusters and metal NPs are very different due to their distinct electronic structures. For comparison, we have prepared a Pt/MCM-22-imp sample with 0.2 wt% of Pt by a conventional impregnation method (see **Methods**). As shown in **Figure S13**, Pt NPs with size of 1~5 nm are formed on MCM-22. The fluorescence emission spectra under excitation at 260 nm (see **Figure 3c**) show that Pt@MCM-22 with Pt clusters present a clear emission peak around 360 nm which can be associated to Pt clusters with less than 10 atoms.^{31,32} In contrast, no fluorescence emission signal can be observed in Pt/MCM-22-imp. The fluorescence emission of Pt clusters can also be seen from the pictures of the two samples under white light and UV light, respectively. As shown in **Figure 3e**, strong fluorescent light emission can be observed in Pt@MCM-22 sample under UV light.

To compare the different properties of subnanometric Pt species in Pt@MCM-22 and Pt NPs in Pt/MCM-22-imp on H₂ activation, H₂-D₂ exchange experiments were carried out.³³ Notice that H₂ can diffuse through the 8-MR window that communicate the supercages in where a portion of Pt species are encapsulated. The results given in **Figure 3d** show that the formation rate of HD over Pt@MCM-22 is much higher than over Pt/MCM-22-imp, indicating that subnanometric Pt species in Pt@MCM-22 are more active on the H₂ activation than Pt NPs in Pt/MCM-22-imp, which is in agreement with literature.³⁴

In order to investigate the chemical states of Pt species in Pt@MCM-22 and Pt/MCM-22-imp, CO was used as probe molecule for IR spectroscopy. As shown in **Figure 3f**, two CO adsorption bands can be observed, which can be ascribed to CO interacting in lineal and bridge configuration, respectively. The reported CO frequency for Pt species in Pt@MCM-22 are lower than those observed for CO adsorbed in atop positions of Pt nanoparticles supported on MCM-22 and some conventional oxide carriers,^{35,36} which indicates a higher electron donor capacity of the subnanometric Pt species. It was suggested that zeolite matrix can act as electron donor increasing electron density of encapsulated Pt clusters.³⁷ On the other hand, small metal cluster may bear a higher electron charge due to their higher unsaturation degree, while specific supports could modify net electronic charge of the clusters.³⁸

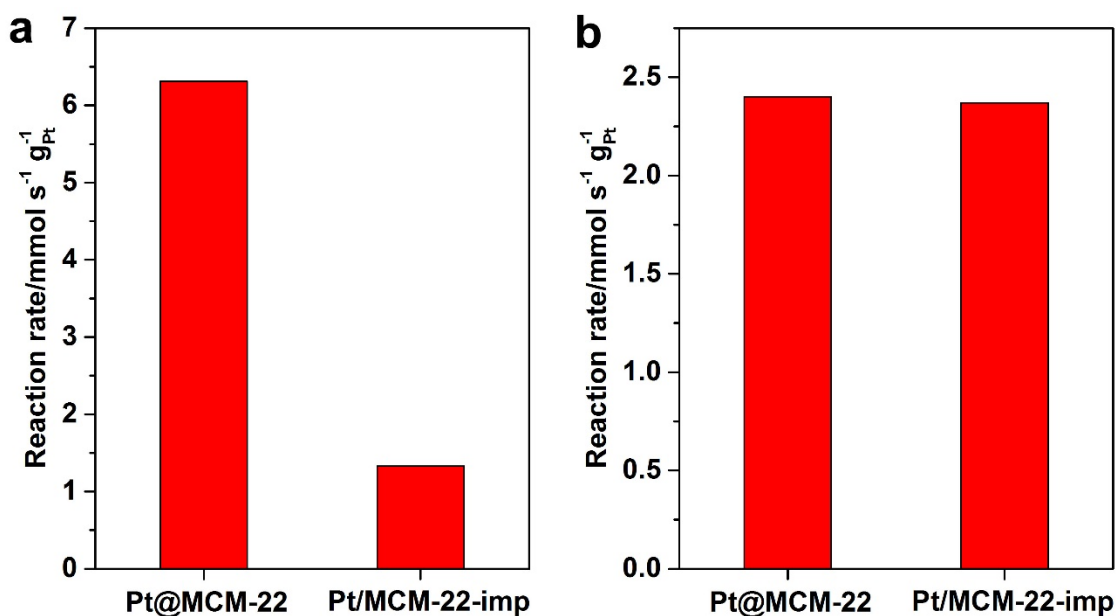


Figure 4| Reaction rates of Pt@MCM-22 and Pt/MCM-22-imp in hydrogenation of light olefins. (a) Hydrogenation of propylene and (b) hydrogenation of isobutene. The reaction rates are normalized based on the amount of Pt species in both catalysts.

Catalytic activity

As it has been presented above, incorporation of Pt in expanded layered precursor of MCM-22 leads to isolated Pt atoms and Pt clusters on the “cups” located at external surface and also probably in the internal space of MCM-22. On the other hand, in the case of Pt/MCM-22-imp sample prepared by impregnation method, most of Pt NPs (1~5 nm) should be only located at the external surface. To test the catalytic properties and to bring more information on the location of Pt species in Pt@MCM-22 sample, we have chosen hydrogenation of alkenes with different molecular sizes as probe reactions. Firstly, the hydrogenation of propylene, which can diffuse through 8-MR windows and reach the supercavities with subnanometric Pt species, was performed in fixed-bed reactor. Results in **Figure 4a** show a higher activity of Pt@MCM-22 than Pt/MCM-22-imp. Notice that the reaction rates of Pt species is about five times higher for Pt@MCM-22. This difference of activity between Pt@MCM-22 and Pt/MCM-22-imp has also been observed before for the H₂-D₂ exchange experiment. The results would confirm the accessibility of propylene to all Pt species regardless of their location within the zeolite. However, as we said before, Pt species can also be encapsulated within 0.7 × 1.8 nm supercavities of MCM-22, which are only accessible through the 8-MR windows. As shown in **Figure**

4b, the reaction rates for hydrogenation of isobutene of Pt/MCM-22-imp is similar to that of Pt@MCM-22, which is contrary to the activity difference for the propylene hydrogenation. Indeed, due to the molecular sieving effect of 8-MR windows in MCM-22, isobutene are only accessible to Pt species located at the external “cups” on the surface of MCM-22 while it should not be accessible to Pt atoms and clusters encapsulated in the cavities inside MCM-22. Therefore, by combining STEM characterization and the catalytic results on hydrogenation of propylene and isobutene, one can speculate that a large part of Pt species are located within the supercavities of MCM-22 in the Pt@MCM-22 sample.

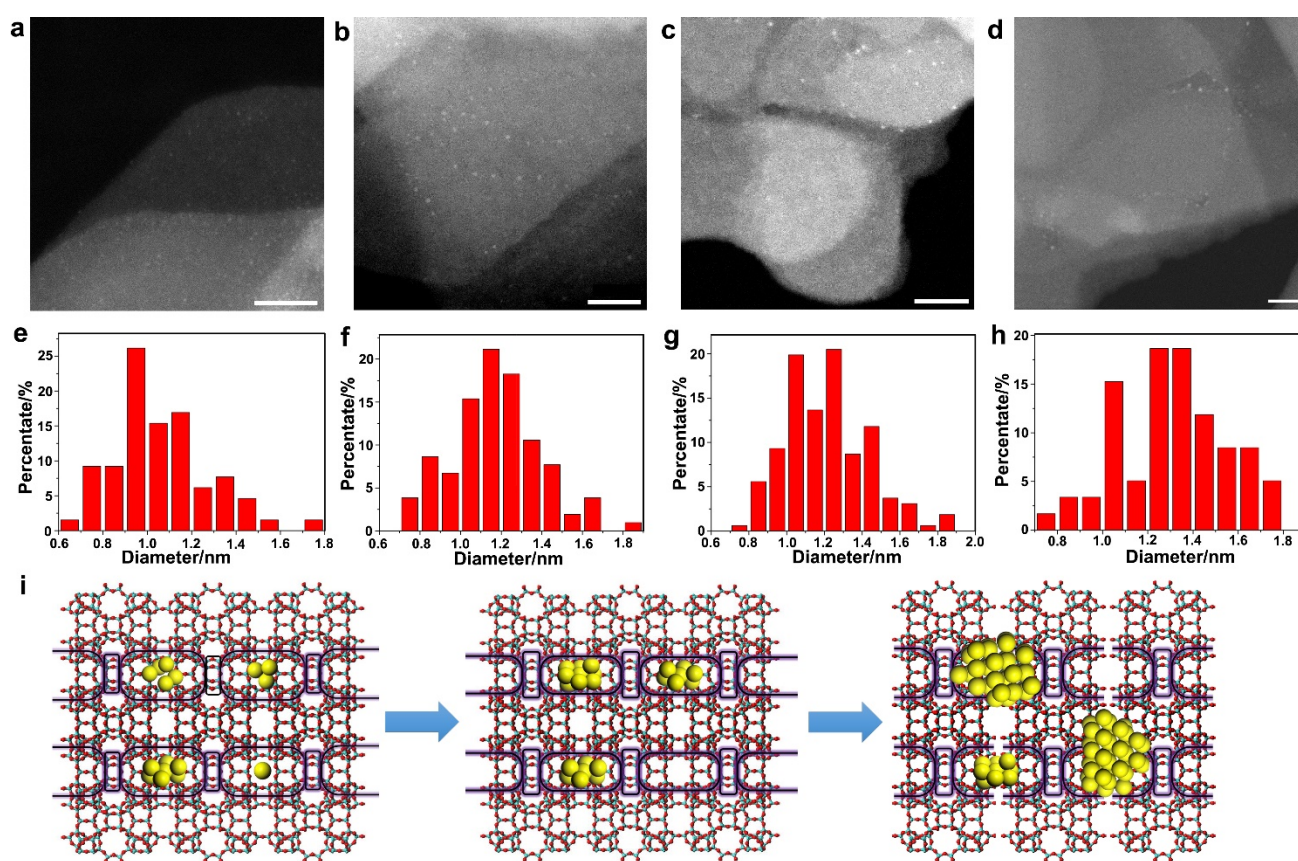


Figure 5| Pt@MCM-22 after high-temperature reduction-oxidation treatments. STEM images of Pt@MCM-22 after different cycles of reduction-oxidation treatments at 650 °C. **a**, Pt@MCM-22-1cycle. **b**, Pt-@MCM-22-2cycles. **c**, Pt-@MCM-22-3cycles. **d**, Pt@MCC-22-4cycles. Scale bar in **a-d**, 20 nm. Size distributions of small Pt nanoparticles in Pt@MCM-22 after different cycles of reduction-oxidation treatments at 650 °C. **e**, Pt@MCM-22-1cycle. **f**, Pt-@MCM-22-2cycles. **g**, Pt-@MCM-2 2-3cycles. **h**, Pt@MCC-22-4cycles. **i**, Schematic illustration of the evolution of Pt

individual atoms and Pt clusters during the high-temperature reduction-oxidation treatments.

High-temperature stability of Pt@MCM-22

The exceptional stability of the subnanometric Pt species in Pt@MCM-22 have been demonstrated by performing reduction-oxidation treatments at 650 °C. Under such harsh conditions, small Pt NPs with size of ~1 nm are formed in Pt@MCM-22 after one cycle of reduction-oxidation treatment at 650 °C (see **Figure 5a** and **Figure S14**). Over 95% percent of Pt species exist as small Pt NPs with size of 1~2 nm. Those individual Pt atoms and small Pt clusters with a few atoms have mostly aggregate to larger Pt clusters, or small Pt NPs (1~2 nm), in Pt@MCM-22. As for Pt clusters with more than 5 atoms, they should be more stable because they are captured by the cups and supercages of MCM-22. Checking by STEM, we have observed some Pt clusters below 1 nm while few Pt individual atoms can be found on in the Pt@MCM-22-1cycle sample (as shown in **Figure S15**). With more cycles of reduction-oxidation treatments, Pt clusters will continue to grow larger, as presented in **Figure 5b** to **Figure 5d** (more STEM images can be found from **Figure S16** to **Figure S18**). Nevertheless, their size distributions (**Figure 5f** to **Figure 5h**) show that most of the small Pt NPs are still below 2 nm, indicating the high stability of Pt species in Pt@MCM-22 during the very extreme reduction-oxidation treatments at 650 °C. In the case of Pt/MCM-22-imp, reduction-oxidation treatments at 650 °C lead to continuous growth of Pt NPs (images are presented from **Figure S19** to **Figure S22** and the size distributions of Pt NPs are shown in **Figure S23**). In the Pt/MCM-22-imp-4cycles sample (**Figure S22**), some Pt NPs as large as 30~50 nm are observed. However, it is important to take into account that, due to the lower melting and boiling point of Pt nanoclusters, subnanometric Pt species can be mobile during the high-temperature treatments, especially for those Pt species located on the external surface.³⁹⁻⁴¹ Thus, after four reduction-oxidation cycles at 650 °C, only ~30% of the initial Pt (measured by ICP) will be remaining in the Pt@MCM-22 sample. Despite that, the stability against agglomeration of Pt species encapsulated in MCM-22 are still much better than the Pt/MCM-22-imp materials prepared through conventional impregnation methods.

Taking into account the higher stability of Pt@MCM-22, we also decide to test its catalytic activity for dehydrogenation of propane. Indeed, dehydrogenation of short alkane molecules is of much interest to activate alkanes and catalytic processes require frequent reaction-regeneration cycles at high

temperature.⁴² As can be seen in **Figure S24**, Pt@MCM-22 exhibits higher activity than Pt/MCM-22-imp at 550 °C. Moreover, after five reaction-regeneration cycles at 550 °C during the catalytic dehydrogenation of propane, Pt@MCM-22 sample retains ~90% of its initial activity while Pt/MCM-22-imp has lost more than 40% of the initial activity. It should be remarked that no significant loss of Pt in Pt@MCM-22 sample is observed by ICP after five cycles of propane dehydrogenation reaction. Then, Pt@MCM-22 sample after two and five reduction-oxidation cycles at 550 °C has also been studied by STEM. As shown in **Figure S25** and **Figure S27**, particle sizes of most of the Pt species slightly increase and still remain below 2 nm. Strong fluorescence emission under UV light can also be observed on those two samples (see **Figure S27**), indicating the presence of Pt clusters even after treatments at 550 °C. This is in agreement with the higher thermal stability of the Pt@MCM-22 sample.

Conclusions

We have presented a new strategy to prepare subnanometric Pt catalysts in 3D MCM-22 zeolite with exceptional high stability, starting from a 2D MWW-type precursors. Pt single atoms and clusters are stable after calcination in air at 540 °C and under reaction conditions. This new method provides a possibility for the generation of highly stable subnanometric metal catalysts for high-temperature catalytic reactions in pure siliceous zeolites.

References

1. Boronat, M., Leyva-Perez, A. & Corma, A. Theoretical and experimental insights into the origin of the catalytic activity of subnanometric gold clusters: attempts to predict reactivity with clusters and nanoparticles of gold. *Acc. Chem. Res.* **47**, 834-844 (2014).
2. Flytzani-Stephanopoulos, M. & Gates, B. C. Atomically dispersed supported metal catalysts. *Ann. Rev. Chem. Bio. Eng.* **3**, 545-574 (2012).
3. Gates, B. C. Supported Metal Clusters: Synthesis, Structure, and Catalysis. *Chem. Rev.* **95**, 511-522 (1995).
4. Corma, A. et al. Exceptional oxidation activity with size-controlled supported gold clusters of low atomicity. *Nat. Chem.* **5**, 775-781 (2013).
5. Yang, M. et al. Catalytically active Au-O(OH)_x-species stabilized by alkali ions on zeolites and mesoporous oxides. *Science* **346**, 1498-1501(2014).
6. Rivallan, M. et al. Platinum sintering on H-ZSM-5 followed by chemometrics of CO adsorption and 2D pressure-jump IR spectroscopy of adsorbed species. *Angew. Chem. Int. Ed.* **49**, 785-789 (2010).
7. Zecevic, J., van der Eerden, A. M., Friedrich, H., de Jongh, P. E. & de Jong, K. P. Heterogeneities of the nanostructure of platinum/zeolite Y catalysts revealed by electron tomography. *ACS Nano* **7**, 3698-3705

- (2013).
8. Philippaerts, A. *et al.* Unprecedented shape selectivity in hydrogenation of triacylglycerol molecules with Pt/ZSM-5 zeolite. *Angew. Chem. Int. Ed.* **50**, 3947-3949 (2011).
 9. Kim, J., Kim, W., Seo, Y., Kim, J.-C. & Ryoo, R. n-Heptane hydroisomerization over Pt/MFI zeolite nanosheets: Effects of zeolite crystal thickness and platinum location. *J. Catal.* **301**, 187-197 (2013).
 10. Goel, S., Wu, Z., Zones, S. I. & Iglesia, E. Synthesis and catalytic properties of metal clusters encapsulated within small-pore (SOD, GIS, ANA) zeolites. *J. Am. Chem. Soc.* **134**, 17688-17695 (2012).
 11. Choi, M., Wu, Z. & Iglesia, E. Mercaptosilane-assisted synthesis of metal clusters within zeolites and catalytic consequences of encapsulation. *J. Am. Chem. Soc.* **132**, 9129-9137 (2010).
 12. Choi, M., Yook, S. & Kim, H. Hydrogen Spillover in Encapsulated Metal Catalysts: New Opportunities for Designing Advanced Hydroprocessing Catalysts. *ChemCatChem* **7**, 1048-1057 (2015).
 13. Kulkarni, A., Lobo-Lapidus, R. J. & Gates, B. C. Metal clusters on supports: synthesis, structure, reactivity, and catalytic properties. *Chem. Comm.* **46**, 5997-6015 (2010).
 14. Guzman, J. & Gates, B. C. Supported molecular catalysts: metal complexes and clusters on oxides and zeolites. *Dalton Trans.*, 3303-3318 (2003).
 15. Leonowicz, M. E., Lawton, J. A., Lawton, S. L. & Rubin, M. K. MCM-22: A Molecular Sieve with Two Independent Multidimensional Channel Systems. *Science* **264**, 1910-1913 (1994).
 16. Cambor, M. A. *et al.* A New Microporous Polymorph of Silica Isomorphous to Zeolite MCM-22. *Chem. Mater.* **8**, 2415-2417 (1996).
 17. Hyotanishi, M., Isomura, Y., Yamamoto, H., Kawasaki, H. & Obora, Y. Surfactant-free synthesis of palladium nanoclusters for their use in catalytic cross-coupling reactions. *Chem. Comm.* **47**, 5750-5752 (2011).
 18. Duchesne, P. N. & Zhang, P. Local structure of fluorescent platinum nanoclusters. *Nanoscale* **4**, 4199-4205 (2012).
 19. Lu, J., Aydin, C., Browning, N. D. & Gates, B. C., Imaging isolated gold atom catalytic sites in zeolite NaY. *Angew. Chem. Int. Ed.* **51**, 5842-5846 (2012).
 20. *Advanced Transmission Electron Microscopy: Applications to Nanomaterials*, Eds. Francis, L., Mayoral, A., and Arenal, R. Springer (2015).
 21. Jena, P.; S. N. Khanna, S. N.; Rao, B. K. *Physics and Chemistry of Finite Systems: From Clusters to Crystals*, 1992, Springer Netherlands.
 22. J Yamasaki *et al*, *Ultramicroscopy* **151**, 224-231 (2015).
 23. K. Sohlberg, T.J. Pennycook, W. Zhou and S.J. Pennycook, Insights into the physical chemistry of materials from advances in HAADF-STEM, *Phys. Chem. Chem. Phys.* **17**, 3982-4006 (2015).
 24. Aydin, C., Lu, J., Browning, N. D. & Gates, B. C. A "smart" catalyst: sinter-resistant supported iridium clusters visualized with electron microscopy. *Angew. Chem. Int. Ed.* **51**, 5929-5934 (2012).
 25. Wei, H. *et al.* FeOx-supported platinum single-atom and pseudo-single-atom catalysts for chemoselective hydrogenation of functionalized nitroarenes. *Nature Comm.* **5**, 5634 (2014).
 26. Addou, R. *et al.* Influence of hydroxyls on Pd atom mobility and clustering on rutile TiO₂(011)-2x1. *ACS Nano* **8**, 6321-6333 (2014).
 27. Jung, U. *et al.* Comparative in Operando Studies in Heterogeneous Catalysis: Atomic and Electronic Structural Features in the Hydrogenation of Ethylene over Supported Pd and Pt Catalysts. *ACS Catal.* **5**, 1539-1551 (2015).
 28. Agostini, G. *et al.* Effect of Different Face Centered Cubic Nanoparticle Distributions on Particle Size and Surface Area Determination: A Theoretical Study. *J. Phys. Chem. C* **118**, 4085-4094 (2014).

29. Alexeev, O. & Gates, B. C. EXAFS characterization of supported metal-complex and metal-cluster catalysts made from organometallic precursors. *Top. Catal.* **10**, 273-293 (2000).
30. Fornasini, P. & Grisenti, R. On EXAFS Debye-Waller factor and recent advances. *J. Synchrotron Rad.* **22**, 1242-1257 (2015).
31. Chakraborty, I., Bhui, R. G., Bhat, S. & Pradeep, T. Blue emitting undecaplatinum clusters. *Nanoscale* **6**, 8561-8564 (2014).
32. Zheng, J., Nicovich, P. R. & Dickson, R. M. Highly fluorescent noble-metal quantum dots. *Ann. Rev. Phys. Chem.* **58**, 409-431 (2007).
33. Okrut, A. *et al.* Selective molecular recognition by nanoscale environments in a supported iridium cluster catalyst. *Nat. Nanotech.* **9**, 459-465 (2014).
34. Zhou, C. *et al.* On the Sequential Hydrogen Dissociative Chemisorption on Small Platinum Clusters: A Density Functional Theory Study. *J. Phys. Chem. C* **111**, 12773-12778 (2007).
35. De La Cruz, C. & Sheppard, N. An exploration of the surfaces of some Pt/SiO₂ catalysts using CO as an infrared spectroscopic probe. *Spectr. Acta A: Mol. Spectr.* **50**, 271-285 (1994).
36. Klünker, C., Balden, M., Lehwald, S. & Daum, W. CO stretching vibrations on Pt(111) and Pt(110) studied by sum frequency generation. *Surf. Sci.* **360**, 104-111 (1996).
37. Stakheev, A. Y., Shpiro, E. S., Jaeger, N. I. & Schulz-Ekloff, G. Electronic state and location of Pt metal clusters in KL zeolite: FTIR study of CO chemisorption. *Catal. Lett.* **32**, 147-158 (1995).
38. Heiz, U., Sanchez, A., Abbet, S. & Schneider, W. D. Catalytic Oxidation of Carbon Monoxide on Monodispersed Platinum Clusters: Each Atom Counts. *J. Am. Chem. Soc.* **121**, 3214-3217 (1999).
39. Levitas, V. I. & Samani, K. Size and mechanics effects in surface-induced melting of nanoparticles. *Nat. Commun.* **2**, 284 (2011).
40. Jiang, H., Moon, K.-s., Dong, H., Hua, F. & Wong, C. P. Size-dependent melting properties of tin nanoparticles. *Chem. Phys. Lett.* **429**, 492-496 (2006).
41. Nanda, K. K., Kruis, F. E. & Fissan, H. Evaporation of Free PbS nanoparticles: Evidence of the Kelvin Effect. *Phys. Rev. Lett.* **89**, 89.256103 (2002).
42. Vajda, S. *et al.* Subnanometre platinum clusters as highly active and selective catalysts for the oxidative dehydrogenation of propane. *Nature Mater.* **8**, 213-216 (2009).

Acknowledgement

This work was funded by the Spanish Government (Consolider Ingenio 2010-MULTICAT (CSD2009-00050) and MAT2014-52085-C2-1-P) and by the Generalitat Valenciana (Prometeo). The Severo Ochoa program (SEV-2012-0267) is thankfully acknowledged. L.L. thanks ITQ for a contract. The authors also thank Microscopy Service of UVP for the TEM and STEM measurements. The HAADF-HRSTEM works have been conducted in the Laboratorio de Microscopias Avanzadas (LMA) at the Instituto de Nanociencia de Aragon (INA)-Universidad de Zaragoza (Spain), Spanish ICTS National facility. Some of the research leading to these results has received funding from the European Union Seventh Framework Program under Grant Agreement 312483-ESTEEM2 (Integrated Infrastructure

Initiative-I3). R.A. also acknowledges funding from the Spanish Ministerio de Economía y Competitividad (FIS2013-46159-C3-3-P).

Author Contributions

A.C. conceived the project, directed the study and wrote the manuscript. L.L. carried out the synthesis, characterizations and catalytic measurements and collaborated in writing the manuscript. U.D. participated in the synthesis and characterization of the materials. R.A. performed the high-resolution STEM characterizations. G.A. performed the XAS measurement and analyzed the data. P.C. carried out the H-D exchange and CO-IR adsorption experiments. U.D., R.A., G.A. and P.C. also collaborated in writing the manuscript.

Competing financial interests

The authors declare no competing financial interests.

Corresponding author

Correspondence to: **Avelino Corma**

Methods

Preparation of Pt@MCM-22 and Pt/MCM-22-imp

Synthesis of the solution containing Pt clusters. Subnanometric Pt species are prepared by a dimethylformamide (DMF) reduction method. 10 mg Pt(acac)₂ (Platinum(II) acetylacetonate) are dissolved in 40 mL DMF. Then the solution is heated at 140 °C for 16 h.

Synthesis of ITQ-1 and Swelled ITQ-1. ITQ-1 zeolite (IZA code MWW) is the pure silica analog of MCM-22. It can be synthesized using trimethyladamantammonium (TMAda⁺) as structure directing agent in absence of alkali cations, but reproducibility problems appeared. If hexamethyleneimine (HMI) is added as second SDA, the reproducibility of the synthesis, as well as the quality of the materials obtained, are greatly improved. The use of TMAda⁺, HMI and sodium cations allows a fast and highly reproducible synthesis of pure silica ITQ-1.

An example of the procedure for the synthesis of ITQ-1 using TMAda⁺, HMI and Na⁺ cations is as follows: 0.95 g of NaCl are dissolved in 50.70 g of a solution 0.42 M of N,N,N-trimethyl-1-adamantanammonium hydroxide, previously diluted with 21.33 g of water. Then, 2.62 g of hexamethyleneimine are added to this solution, followed by 4.88 g of silica (Aerosil 200, Degussa) under continuous stirring. This reaction mixture is heated in a PTFE lined stainless steel autoclave at 150 °C rotated at 60 rpm for 5 days. After filtering, the white solid obtained is washed until pH was less than 9.

In order to prepare the swelled purely siliceous ITQ-1 with subnanometric Pt species, 2 g of the lamellar precursor was dispersed in 8 g of H₂O milliQ, and 40 g of a cetyltrimethylammonium hydroxide solution (25 wt.%, 50% exchanged Br⁻/OH⁻) and 12 g of a solution of tetrapropylammonium hydroxide (40 wt.%, 30% exchanged Br⁻/OH⁻) were added together with 40 mL of Pt-DMF solution, being the final pH around 12.5. The resultant mixture was heated at 52 °C, stirring vigorously, for 16 hours in order to facilitate the swelling of the layers of the precursor material. At this point, the solid was recovered by centrifugation and washed with distilled water, being dried at 60 °C for 12 hours.

Synthesis of Pt@MCM-22. Pt@MCM-22 can be obtained through the calcination of the Pt@Swelled MWW(P) composite. The calcination process is performed as following. 1) Rising temperature from room temperature to 540 °C with a ramp rate of 2 °C/min in N₂ atmosphere. The total time in N₂ atmosphere is about 4.5 h. 2) Switching the atmosphere to air and keep at 540 °C for 4 h. 3) Cooling

from 540 °C to room temperature in air atmosphere. The obtained sample is denoted as Pt@MCM-22.

Stability test of Pt@MCM-22 samples. In order to test the thermal stability of the subnanometric Pt species, a high-temperature reduction-oxidation cyclic treatment was used. Fresh Pt@MCM-22 sample is firstly sent to reduction treatment at 650 °C in H₂ (temperature ramp rate is 2 °C/min and maintain at 650 °C for 2 h). After reduction treatment, the sample is calcined at 650 °C in air (temperature ramp rate is 2 °C/min and maintain at 650 °C for 2 h). The above reduction and oxidation treatment is considered as one cycle and the sample after one-cycle treatment is called Pt@MCM-22-1cycle. In a similar way, Pt@MCM-22-1cycle can be further treated in consecutive reduction-oxidation cycles.

Preparation of Pt/MCM-22-imp through impregnation method. In order to compare with the Pt@MCM-22 materials, Pt/MCM-22-imp sample was prepared through conventional wet-impregnation method. MCM-22 (prepared through the calcination of ITQ-1) is used as the support. DMF solution containing subnanometric Pt species are used as the precursor for Pt nanoparticles. In a typical preparation of Pt/MCM-22-imp with 0.2 wt.% of Pt, 2.2 g MCM-22 (pure silica) was firstly dispersed in 25 mL of H₂O and 35 mL of Pt-DMF solution. The suspension was kept stirring at room temperature for 30 min and then sent to a silicone oil bath at 120 °C to remove the solvent. After removing the solvent, the solid was dried in air at 100 °C for 16 h. At last, Pt/MCM-22-imp can be obtained after reduction in H₂ at 450 °C (temperature ramp rate is 5 °C/min) for 3 h.

We have also tried to use incipient wetness impregnation (IWI) method to prepare supported Pt nanoparticles on MCM-22. However, the dispersion of Pt obtained by the IWI method does not give better dispersion of Pt species on MCM-22.

Characterizations

Samples for electron microscopy studies were prepared by dropping the suspension of Pt@MCM-22 or other materials using ethanol as the solvent directly onto holey-carbon coated Cu grids. The measurements were performed using a JEOL 2100F microscope operating at 200 kV both in transmission (TEM) and scanning-transmission modes (STEM). STEM images were obtained using a High Angle Annular Dark Field detector (HAADF), which allows Z-contrast imaging. The current density is 0.9 pA/cm² when working on JEOL 2100F. High-resolution STEM (HRSTEM) imaging,

using the HAADF detector, was performed using a FEI Titan Low-Base microscope operated at 300 kV and equipped with a Cs probe corrector (CESCOR from CEOS GmbH), a monochromator and an ultra-bright X-FEG electron source. The convergence angle was 25 mrad and the inner and outer angles for HAADF imaging were 70 and 200 mrad, respectively. The typical probe current was set to 2 pA and the total dose on the sample varied between $\sim 0.2\text{-}3\text{ C/cm}^2$ under the HRSTEM imaging conditions, which corresponds to low-dose conditions. [1] Multi-slice HRSTEM-HAADF image simulations have been carried out using QSTEM software [2], with the experimental settings of the FEI Titan Low Base as inputs. For this purpose, the thermal diffuse scattering parameter was fixed at 30 for a temperature of 300 K.

Hydrogen/deuterium ($\text{H}_2\text{-D}_2$) exchange experiments were carried out in a flow reactor at room temperature (25 °C). The formation rate of HD species can be measured by the enhancement of the mass signal intensity (ion current). The feed gas consisted of 4 mL/min H_2 , 4 mL/min D_2 and 18 mL/min argon, and the total weight of catalyst was 115 mg. The sample has been diluted with 230 mg of SiC. Reaction products (H_2 , HD and D_2) were analysed with a mass spectrometer (Omnistar, Balzers). The m/z mass used are 2 for H_2 , 4 for D_2 and 3 for HD. The sample was in situ reduced at 200 °C for 2 h with a temperature-rising rate of 10 °C/min from room temperature to 200 °C. Then the temperature was decreased to 25 °C and, once stabilized, the H_2 feed was changed to the reactant gas composition. The temperature was maintained at 25 °C for about 60 minutes.

Powder X-ray diffraction (XRD) was performed with a HTPhilips X'Pert MPD diffractometer equipped with a PW3050 goniometer using Cu $K\alpha$ radiation and a multisampling handler.

XAS measurements were carried out on the BM23 beamline at ESRF facility (Grenoble, France). Fluorescence XAS spectra at the Pt L_3 -edge (11.564 keV) were collected with a 13-element Ge detector on self-supported pellet at room temperature, Pt reference foil was collected for energy calibration. The beam energy were selected by double-crystal Si(111) monochromator, third harmonic rejection was performed by Rh coated mirror with an angle of -4 mrad. [3]. EXAFS signal were extracted and analyzed by IFEFFIT package [4].

References:

[1] Ortalan, V., Uzun, A., Gates, B. C. & Browning, N. D. Direct imaging of single metal atoms and clusters in the pores of dealuminated HY zeolite. *Nat. Nanotechnol.* 5, 506-510 (2010).

[2] C. Koch, 2002, PhD Thesis: Arizona State University.

[3] Mathon, O. *et al.* The time-resolved and extreme conditions XAS (TEXAS) facility at the European Synchrotron Radiation Facility: the general-purpose EXAFS bending-magnet beamline BM23. *J. Synchrotron Rad.* **22**, 1548-1554 (2015).

[4] Newville, M. IFEFFIT: interactive XAFS analysis and FEFF fitting. *J. Synchrotron Rad.* **8**, 322-324 (2001).

Measurement of catalytic performance of Pt@MCM-22 and Pt/MCM-22-imp.

Hydrogenation of propylene to propane. Hydrogenation of propylene was performed in a flow fixed-bed continuous reactor. 30 mg Pt@MCM-22 diluted with 2 g SiC (the grain size of SiC used in this work is between 0.4 to 0.6 mm) powder was loaded in a quartz tube reactor. The reaction was performed at room temperature with a flow of 2 mL/min of propylene, 6 mL/min of H₂ and 32.7 mL of Ar. Products were analyzed with a Bruker on-line GC with FID detector. The conversion of C₃H₆ was kept below 15 % to calculate the reaction rates.

Hydrogenation of isobutene to isobutane. Hydrogenation of isobutene was performed in a flow fixed-bed continuous reactor. 30 mg Pt@MCM-22 diluted with 2 g SiC powder was loaded in a quartz tube reactor. The reaction was performed at room temperature with a flow of 1.5 mL/min of isobutene, 4.5 mL/min of H₂ and 24 mL of Ar. Products were analyzed by Bruker on-line GC with FID detector. The conversion of isobutene was kept below 15 % when calculating reaction rates.

Dehydrogenation of propane to propylene. Dehydrogenation of propane was performed in a fixed-bed reactor. A cylindrical quartz tube was loaded with 1.10 g of Pt@MCM-22 catalyst material (In the case of Pt/MCM-22-imp, the amount of catalyst was 0.60 g). Catalyst was diluted with SiC to keep the total volume of solid constant (3 cm³). Before the reaction, the sample was reduced by H₂ at 550 °C. The reaction was run at 550 °C with a flow of 30 mL/min of propane and 3 mL/min of N₂ for 15 min, followed by a regeneration step at 550 °C with a flow of air for 30 min. The reaction stream was analyzed by an on-line Varian GC, which was equipped with a flame ionization detector (FID) and a thermal conductivity detector (TCD). Conversion of C₃H₈ was kept below 10 % to calculate the initial reaction rate.